Tailoring the Phase and Power Flow of Electromagnetic Fields

Gurkan Gok and Anthony Grbic*

Department of Electrical Engineering and Computer Science, University of Michigan, Ann Arbor, Michigan 48109-2122, USA

(Received 27 June 2013; published 6 December 2013)

A method for arbitrarily controlling the phase progression and power flow of electromagnetic fields within a region of space is introduced. Specifically, we describe how a 2D inhomogeneous, anisotropic medium can be designed that supports desired spatial distributions of the wave vector and Poynting vector direction. Plane-wave relations in anisotropic media are used in conjunction with an impedance matching process to find the required material parameters. The developed formulation allows one to independently tailor the phase and amplitude of a field profile. The work will find application in the design of electromagnetic or optical guiding structures and radiating apertures.

DOI: 10.1103/PhysRevLett.111.233904 PACS numbers: 41.20.Jb, 42.25.Bs, 42.60.Jf, 42.79.−e

It is well known that an anisotropic material can support electromagnetic propagation with phase progression and power flow in different directions [1]. This simple fact suggests that a carefully designed medium, which is anisotropic and spatially inhomogeneous, can tailor phase and power flow as a function of position. In such a medium, anisotropy controls the local phase and power flow, while the inhomogeneity allows spatial variation. This spatial control of electromagnetic fields can be used to independently tailor the phase and amplitude of a field profile.

Transformation electromagnetics [2,3] has provided a prescription for finding the material parameters needed for such field manipulation [4–7]. In transformation electromagnetics, a desired field distribution is derived from an initial one through a coordinate transformation, from which the spatial distribution of material parameters are computed. However, finding the coordinate transformation that yields the field of interest is not always intuitive, straightforward, or necessarily possible.

In this work, a different design approach is introduced. Material parameters are defined in terms of the phase progression and power flow [8] within a region of space (the transformation region), that is embedded within a surrounding medium. First, spatial distributions of the wave vector ($\vec{k}$) and Poynting vector ($\vec{S}$) direction are stipulated within the transformation region. From these two distributions, the required anisotropic, inhomogeneous material parameters needed to support such propagation are found. Plane-wave relations in anisotropic media are used along with an impedance matching process (which minimizes intercell reflections) to find the desired material tensors. An additional condition is also imposed on the material parameters of the transformation region to ensure it is impedance matched to the surrounding medium for all illuminations. This condition stipulates that the determinant of the region's material tensors is equal to that of the surrounding medium.

A few simplifying assumptions are made in finding the material parameters of the anisotropic inhomogeneous transformation region. In the design approach, it is assumed that (a) the region is discretized into unit cells that are much smaller than the guided wavelength and (b) the discretized cells are displaced (not in the extreme near field) from a localized source. This allows the electromagnetic field within each cell to be treated locally as a plane wave.

The proposed design approach provides independent spatial control of phase progression and power flow. It could find use in the design of a wide range of electromagnetic devices including antennas and beam-forming networks, and may also find application in scattering control [9,10] and holography [11,12]. In addition, the method could provide a novel approach to signal routing, the design of mode conversion devices [13], and the generation of extreme antenna apertures for superdirective radiation [14] or the excitation of Airy [15–18] and Bessel beams [19–22]. For example, in antenna design, one may wish to control power flow across an aperture in order to realize a given amplitude distribution (beam shape), while at the same time control phase progression to establish a certain beam-pointing direction. In the case of a beam former, one may wish to stipulate an input field distribution (excitation) and an output field distribution (amplitude and phase distribution of the antenna elements), with a transition from one to the other. Therefore, spatial control of phase and power flow also allows one to independently mold the phase and amplitude of a field profile. Earlier works have attempted to control these two quantities through coordinate transformations. The finite embedded coordinate transformation method introduced in [23] was used to laterally displace the power flow of an Gaussian beam while preserving its phase progression. On the other hand [24], showed how to control the phase front of a beam while retaining its power flow direction. Here, we demonstrate simultaneous control over both the phase progression and power flow of electromagnetic fields without defining a coordinate transformation.

For simplicity, the proposed design approach is applied to a 2D medium. In particular, a TM_z polarization is

considered (a TE_z formulation can be derived using duality). Therefore, the nonzero field quantities are the magnetic field in the x and y directions (H_x and H_y) and the electric field in the z direction (E_z). At each point in space, the relevant material parameters are a 2×2 relative permeability tensor in the x-y plane and a scalar relative permittivity in the z direction

$$\bar{\bar{\mu}} = \begin{bmatrix} \mu_{xx} & \mu_{xy} \\ \mu_{yx} & \mu_{yy} \end{bmatrix}, \qquad \epsilon = \epsilon_z. \tag{1}$$

We will first review plane-wave relations in an anisotropic, homogeneous medium, and then use them to define material parameters in terms of the local wave vector $\vec{k}$, the direction of the Poynting vector $\vec{S}$, and the permittivity constant ϵ_z. For the polarization of interest, Maxwell's time-harmonic equations for plane waves are

$$-j\vec{k} \times \vec{E} = -j\omega \bar{\bar{\mu}} \mu_o \vec{H}, \quad -j\vec{k} \times \vec{H} = j\omega \epsilon_z \epsilon_o \vec{E}. \tag{2}$$

Considering only the nonzero field quantities, these two vector equations can be rewritten as

$$\begin{bmatrix} \bar{k}_y \\ \bar{k}_x \end{bmatrix} = \begin{bmatrix} \mu_{xx} & -\mu_{xy} \\ -\mu_{yx} & \mu_{yy} \end{bmatrix} \begin{bmatrix} \bar{\eta}_y^{-1} \\ \bar{\eta}_x^{-1} \end{bmatrix} \tag{3}$$

$$\epsilon_z = \begin{bmatrix} \bar{k}_x & \bar{k}_y \end{bmatrix} \begin{bmatrix} \bar{\eta}_x^{-1} \\ \bar{\eta}_y^{-1} \end{bmatrix}, \tag{4}$$

where $\bar{\eta}_x = -(1/\eta_o)(E_z/H_y)$, $\bar{\eta}_y = (1/\eta_o)(E_z/H_x)$ are the wave impedances and $\bar{k}_x = k_x/k_o$, $\bar{k}_y = k_y/k_o$ are the wave numbers in the x and y directions, normalized with respect to their free space values. Using (4), the wave impedances can be written in terms of the wave numbers, the ratio $\kappa = \bar{\eta}_x/\bar{\eta}_y$, and the permittivity constant

$$\bar{\eta}_x = \frac{\bar{k}_x + \kappa \bar{k}_y}{\epsilon_z}, \qquad \bar{\eta}_y = \frac{\bar{k}_x + \kappa \bar{k}_y}{\kappa \epsilon_z}. \tag{5}$$

The ratio κ defines the direction (θ_s) of $\vec{S}$ with respect to the x axis: $\kappa = \tan(\theta_s)$. Therefore, if $\vec{k} = k_x\hat{x} + k_y\hat{y}$ and the ratio κ are given at a point in space, the wave impedances are defined by the local permittivity. Expressions for the permeability tensor can also be written using (3) and (4) as

$$\bar{\bar{\mu}} = \begin{bmatrix} \frac{\bar{k}_y}{\epsilon_z}\left(\frac{\bar{k}_x}{\kappa} + \bar{k}_y\right) + \frac{\mu_{xy}}{\kappa} & \mu_{xy} \\ \mu_{yx} & \frac{\bar{k}_x}{\epsilon_z}(\bar{k}_x + \kappa \bar{k}_y) + \mu_{yx}\kappa \end{bmatrix}, \tag{6}$$

where μ_{xy} and μ_{yx} can be chosen arbitrarily, while still ensuring the specified phase and power flow. If it is further assumed that the permeability tensor $\bar{\bar{\mu}}$ is symmetric and its determinant is equal to that of the surrounding medium's (assumed to be free space) permeability $\bar{\bar{\mu}}_s$

$$|\bar{\bar{\mu}}| = |\bar{\bar{\mu}}_s| = 1, \tag{7}$$

the expressions for the permeability tensor simplify to

$$\bar{\bar{\mu}} = \begin{bmatrix} \frac{\epsilon_z}{(\bar{k}_x + \kappa \bar{k}_y)^2} + \frac{\bar{k}_y^2}{\epsilon_z} & \frac{\kappa \epsilon_z}{(\bar{k}_x + \kappa \bar{k}_y)^2} - \frac{\bar{k}_x \bar{k}_y}{\epsilon_z} \\ \frac{\kappa \epsilon_z}{(\bar{k}_x + \kappa \bar{k}_y)^2} - \frac{\bar{k}_x \bar{k}_y}{\epsilon_z} & \frac{\kappa^2 \epsilon_z}{(\bar{k}_x + \kappa \bar{k}_y)^2} + \frac{\bar{k}_x^2}{\epsilon_z} \end{bmatrix}. \tag{8}$$

The condition on the determinant of the permeability tensor is an inherent property of transformation electromagnetics designs that operate in free space. It ensures that the transformed region (device) remains impedance matched to its surrounding medium under all plane-wave excitations. Therefore, if $\vec{k}$ and κ are stipulated, (8) shows that the local permittivity constant defines the local permeability tensor.

Using the expressions for the wave impedances (5) and permeability entries (8), a systematic design procedure for finding the material parameters needed to support arbitrary spatial distributions of phase and power flow will be introduced. The design procedure allows the material parameters of the anisotropic, inhomogeneous transformation region to be found. To find the material parameters, the two-dimensional transformation region is discretized into a grid of unit cells, as shown in Fig. 1(a). Here, a simple square grid is considered. Next, the $\vec{k}$ and direction of $\vec{S}$ are stipulated at the center of each unit cell, defining the phase and power flow within the discretized space [see Fig. 1(a)]. From these two spatial distributions, the permeability of the unit cells can be written in terms of each cell's permittivity using (8). Therefore, the unknowns to be solved for become the unit cell permittivities. They can be found through an impedance matching process in which the wave impedances, given by (5), of adjacent unit cells are matched. Once the permittivities are found through this process, the permeability entries can be computed using (8).

A rigorous optimization method for finding the optimal permittivity distribution that impedance matches adjacent cells is described in the Supplemental Material [25]. The optimization process adjusts the permittivities of all unit cells to minimize intercell reflections. For designs

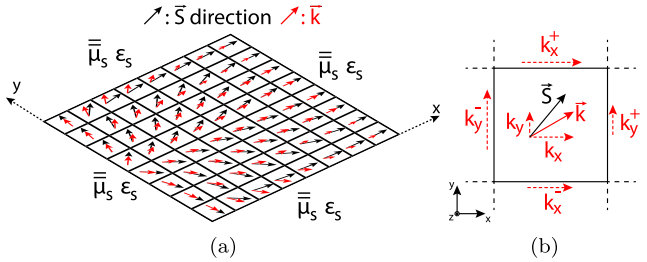

FIG. 1 (color online). (a) The transformation region embedded within a surrounding medium. The transformation region is discretized into unit cells, with the wave vector $\vec{k}$ and direction of $\vec{S}$ stipulated at the center of each cell. (b) A unit cell of the transformation region. The wave numbers along the edges of the cell are shown.

where there are input and desired output field distributions, a linear transition in wave impedances between the input and output can be used to find the permittivity distribution instead of an optimization process. According to (5), the permittivity of a unit cell can be calculated from one of its wave impedances, $\bar{\eta}_x$ or $\bar{\eta}_y$, if $\vec{k}$ and κ are specified. This simple technique will be used to find the permittivity distributions for the design examples presented in the Letter. As noted earlier, once the permittivity values of the unit cells are found, the permeability tensor is calculated using (8). Because of (7), the inhomogeneous, anisotropic transformation region remains impedance matched to its surrounding medium under different excitations.

To demonstrate the potential of the described approach for controlling electromagnetic fields, a couple illustrative examples will be shown. Let us consider a vertical electric current source radiating in an isotropic medium with relative material parameters: $\mu_s = 1$, $\epsilon_s = 1$. In the examples, the source's field will be reshaped over the transformation region, denoted by the dashed lines in Fig. 3(a). The transformation region is discretized into 10×60 square unit cells. The unit cell dimension is assumed to be $d = \lambda_0/7.2$ (4.2 mm) at an operating frequency of 10 GHz, which results in a transformation region that is $1.4\lambda_0 \times 8.4\lambda_0$. The cylindrical source is located 10 unit cells from the input boundary [boundary 1 shown in Fig. 3(a)].

Through these examples, we will demonstrate arbitrary spatial control of the wave vector and Poynting vector direction within the transformation region. Such control over electromagnetic fields will be used to transform the incident field at input boundary 1 to a desired field (amplitude and phase) distribution at output boundary 2 [see Fig. 3(a)].

A few things need to be said about defining the phase progression and power flow within the transformation region. In general, the phase progression must be physical. The difference in wave numbers between a unit cell's y-directed edges ($\Delta k_y = k_y^+ - k_y^-$) must be equal to the difference in wave numbers between its x-directed edges ($\Delta k_x = k_x^+ - k_x^-$), as shown in Fig. 1(b). In other words, the phase delay around the cell edges must sum to zero: $k_y^- + k_x^+ - k_y^+ - k_x^- = 0$. The wave vector at the center of each unit cell can be found by averaging the wave numbers along the x- and y- directed edges separately: $\vec{k} = (k_x^+ + k_x^-)\hat{x}/2 + (k_y^+ + k_y^-)\hat{y}/2$. In contrast, the Poynting vector direction at the center of each unit cell can be set arbitrarily.

In the examples that follow, phase progression within the transformation region is systematically defined. The wave number k_y along the input boundary [boundary 1 in Fig. 3(a)] is dictated by the cylindrical excitation, given that the transformation region is reflectionless. The wave number k_y along all other y-directed unit cell edges is assigned, assuming the input phase distribution (k_y variation) at boundary 1 transitions linearly through the transformation region to the output phase distribution at boundary 2. The wave number k_x along boundary 3 is assigned arbitrarily. The wave number k_x along all other x-directed cell edges is then found using the relation $\Delta k_x = \Delta k_y$.

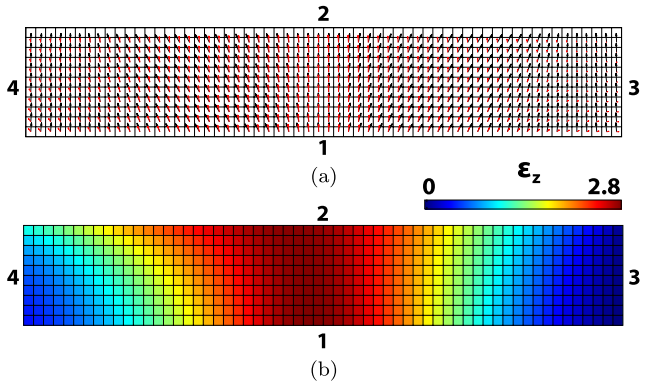

FIG. 2 (color online). (a) Spatial distributions of $\vec{k}$ and direction of $\vec{S}$ that establish a trapezoidal power density and linear phase profile along boundary 2. (b) Calculated permittivity distribution assuming a linearly tapered wave impedance, $\bar{\eta}_x$, from boundary 1 to boundary 2.

The Poynting vector direction for cells along boundary 1 is dictated by the cylindrical excitation. Linear power flow through the transformation region is assumed when mapping the input power density at boundary 1 to the output power density at boundary 2. A detailed discussion of the linear power density mapping is provided in [25]. The mapping allows the Poynting vector direction to be determined at the center of each unit cell within the

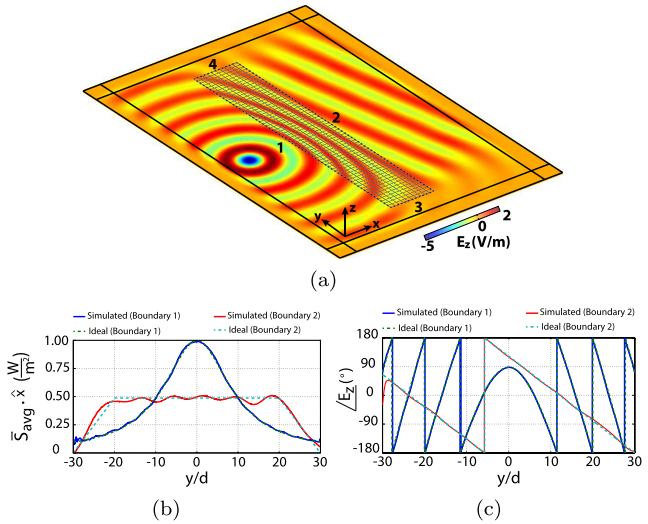

FIG. 3 (color online). (a) Time snapshot of the simulated, vertical electric field (E_z) within the transformation region of the design shown in Fig. 2. (b) Simulated and ideal power densities along boundary 1 and boundary 2. (c) Phase profiles along boundary 1 and boundary 2. $y = 0$ corresponds to the center of the transformation region.

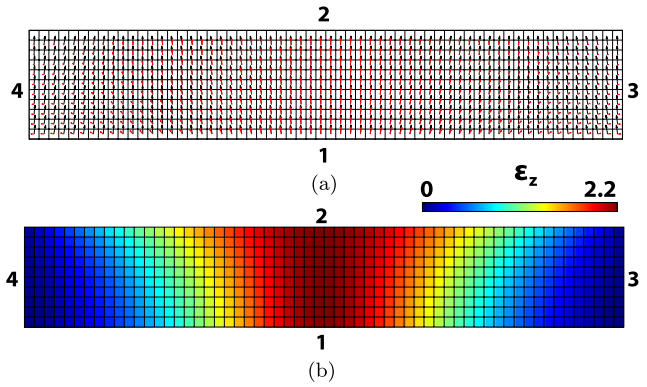

FIG. 4 (color online). (a) Spatial distributions of $\vec{k}$ and direction of $\vec{S}$ that establish a triangular power density and uniform phase profile along boundary 2. (b) Calculated permittivity distribution assuming a linearly tapered wave impedance $\bar{\eta}_x$ from boundary 1 to boundary 2.

transformation region. Further, the power through the input and output boundaries is assumed to be equal, in order to eliminate power leakage through the sides (boundaries 3 and 4) of the transformation region. The permittivity distribution in the transformation region is calculated using (5) from the wave vector and power flow distributions and $\bar{\eta}_x$, which is linearly tapered from boundary 1 to boundary 2. It should be pointed out that linear power flow and a linear phase transition from the input to the output field profiles is assumed for simplicity. These are only one set of an infinite number of possibilities.

First, let us consider an example where the transformation region produces a trapezoidal power density and linear

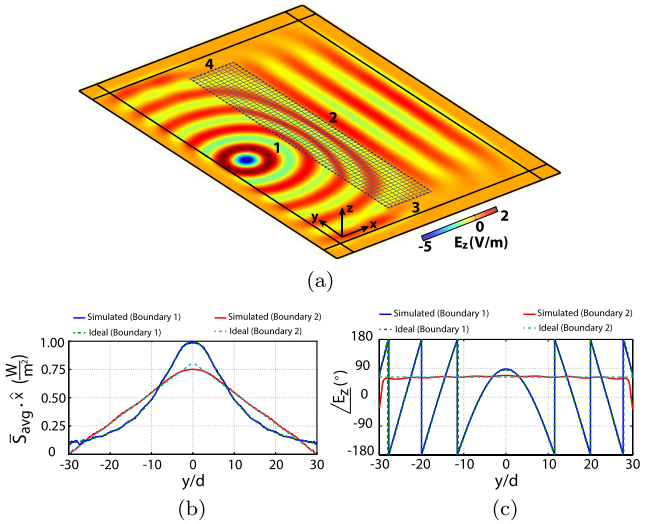

FIG. 5 (color online). (a) Time snapshot of the simulated, vertical electric field (E_z) within the transformation region of the design shown in Fig. 4. (b) Simulated and ideal power densities along boundary 1 and boundary 2. (c) Phase profiles along boundary 1 and boundary 2. $y = 0$ corresponds to the center of the transformation region.

phase progression at boundary 2. Specifically, a wave number of $k_y = 0.20k_o$ is chosen along the boundary 2, and a wave number of $k_x = 0$ along boundary 3. Figure 2(a) shows the assigned $\vec{k}$ and direction of $\vec{S}$ vectors with red and black arrows, respectively. The calculated permittivity distribution is shown in Fig. 2(b). The permeability tensor of each unit cell is found by substituting the vector distributions of Fig. 2(a) and the permittivity values of Fig. 2(b) into (8). A time snapshot of the simulated, vertical electric field (E_z) is shown in Fig. 3(a). A beam emerging from boundary 2 at an angle of 12° with respect to the x axis is observed, verifying that the phase progression along boundary 2 is $k_y = 0.20k_o$. Figures 3(b) and 3(c) plot the ideal (stipulated) and simulated power density and phase profiles at boundaries 1 and 2. Close agreement is shown. An additional design example demonstrating a trapezoidal output power density and uniform phase is provided in the Supplemental Material [25]. All electromagnetic simulations were performed using COMSOL MULTIPHYSICS, a commercial finite element electromagnetic solver.

In the second example, a transformation region is designed to produce a triangular power density distribution and uniform phase at boundary 2. Zero phase progression ($k_y = 0$) is assumed along boundary 2, and a wave number of $k_x = 0$ along boundary 3. Figure 4(a) shows the assigned $\vec{k}$ and direction of $\vec{S}$ vectors with red and black arrows, respectively. The required permittivity distribution is plotted in Fig. 4(b). The permeability tensor of each unit cell is found as in the previous example. A time snapshot of the simulated, vertical electric field is shown in Fig. 5(a). A beam emerging from boundary 2 in the normal direction verifies the desired phase progression along boundary 2: $k_y = 0$. In Figs. 5(b) and 5(c), the ideal and simulated power density and phase profiles at boundaries 1 and 2 are plotted, and show close agreement. The reflectionless performance that results from the matching process can provide a solution to the impedance mismatch observed in electromagnetic wave collimators designed through coordinate transformation [26]. Additional examples showing more extreme output profiles and vector distributions are provided in the Supplemental Material [25].

We have proposed a method for controlling the power flow and phase progression of electromagnetic fields in a two dimensional space. The method enables the design of reflectionless, inhomogeneous, anisotropic media that can support prescribed spatial distributions of the wave vector and Poynting vector direction. This spatial control of phase and power flow allows the amplitude and phase of a field profile to be tailored arbitrarily. Specific examples are reported which show how the proposed method can be used to tailor the field radiated by a cylindrical source into desired amplitude and phase profiles. Metamaterials can be employed to realize the anisotropic, inhomogeneous materials required in the proposed design approach. At microwave and millimeter-wave frequencies, circuit-based

tensor (anisotropic) metamaterials [27,28] are particularly well suited for the implementation of TM_z polarized devices. At optical frequencies, plasmonic or dielectric metamaterials and the concept of nanocircuit elements [29] could be employed. Future work includes extending the proposed method of controlling power flow and phase progression to three dimensions.

This work was supported by a Presidential Early Career Award for Scientists and Engineers (PECASE) Grant No. (FA9550-09-1-0696) and an NSF Faculty Early Career Development Award (ECCS-0747623).

*Corresponding author.
agrbic@umich.edu

[1] A. Yariv and P. Yeh, *Optical Waves in Crystals* (John Wiley & Sons, New York, 1984).
[2] U. Leonhardt, Science **312**, 1777 (2006).
[3] J. B. Pendry, D. Schurig, and D. R. Smith, Science **312**, 1780 (2006).
[4] U. Leonhardt and T. G. Philbin, Prog. Opt. **53**, 69 (2009).
[5] H. Chen, C. T. Chan, and P. Sheng, Nat. Mater. **9**, 387 (2010).
[6] D. H. Kwon and D. H. Werner, IEEE Antennas and Propagation Magazine **52**, 24 (2010).
[7] N. B. Kundtz, D. R. Smith, and J. B. Pendry, Proc. IEEE **99**, 1622 (2011).
[8] G. Gok and A. Grbic, IEEE Trans. Microwave Theory Tech. **61**, 1414 (2013).
[9] D. Sievenpiper, J. Colburn, B. Fong, J. Ottusch, and J. Visher, in *Proceedings of IEEE Antennas and Propagation Society International Symposium (APSURSI)* (IEEE, Washington, DC, 2005), p. 256.
[10] B. H. Fong, J. S. Colburn, J. J. Ottusch, J. L. Visher, and D. F. Sievenpiper, IEEE Trans. Antennas Propag. **58**, 3212 (2010).
[11] P. Hariharan, *Optical Holography: Principles, Techniques and Applications* (Cambridge University Press, Cambridge, England, 1996), p. 11.
[12] P. Checcacci, V. Russo, and A. Scheggi, IEEE Trans. Antennas Propag. **18**, 811 (1970).
[13] M. Yang, J. Li, and K. J. Webb, IEEE Trans. Microwave Theory Tech. **52**, 161 (2004).
[14] S. A. Schelkunoff, Bell Syst. Tech. J. **22**, 80 (1943).
[15] M. V. Berry and N. L. Balazs, Am. J. Phys. **47**, 264 (1979).
[16] G. A. Siviloglou and D. N. Christodoulides, Opt. Lett. **32**, 979 (2007).
[17] G. A. Siviloglou, J. Broky, A. Dogariu, and D. N. Christodoulides, Phys. Rev. Lett. **99**, 213901 (2007).
[18] Y. Hu, G. A. Siviloglou, P. Zhang, N. K. Efremidis, D. N. Christodoulides, and Z. Chen, in *Nonlinear Photonics and Novel Optical Phenomena*, edited by Z. Chen and R. Morandotti (Springer, New York, 2012).
[19] J. Durnin, J. Opt. Soc. Am. A **4**, 651 (1987).
[20] J. Durnin, J. J. Miceli, and J. H. Eberly, Phys. Rev. Lett. **58**, 1499 (1987).
[21] D. McGloin and K. Dholakia, Contemp. Phys. **46**, 15 (2005).
[22] M. Ettore, S. M. Rudolph, and A. Grbic, IEEE Trans. Antennas Propag. **60**, 2645 (2012).
[23] M. Rahm, S. A. Cummer, D. Schurig, J. B. Pendry, and D. R. Smith, Phys. Rev. Lett. **100**, 063903 (2008).
[24] Y. Ke, W. Shu, H. Luo, S. Wen, and D. Fan, J. Europ. Opt. Soc. Rap. Publ. **7**, 12013 (2012).
[25] See Supplemental Material at http://link.aps.org/supplemental/10.1103/PhysRevLett.111.233904 for additional information on the presented method.
[26] D. H. Kwon and D. H. Werner, New J. Phys. **10**, 115023 (2008).
[27] G. Gok and A. Grbic, IEEE Trans. Antennas Propag. **58**, 1559 (2010).
[28] G. Gok and A. Grbic, IEEE Trans. Antennas Propag. **61**, 728 (2013).
[29] N. Engheta, A. Salandrino, and A. Alu, Phys. Rev. Lett. **95**, 095504 (2005).